Topographic Effect on Geostrophic Adjustment and Frontogenesis①

Fang Juan (方 娟) and Wu Rongsheng (伍荣生)

The Key Laboratory of Mesoscale Sever Weather (MOE), Nanjing University, Nanjing 210093

(Received June 2, 2000; revised February 16, 2001)

ABSTRACT

Three conservative principles: potential vorticity, absolute momentum and potential temperature are used to study the influence of topography on the local frontogenesis and geostrophic adjustment, which are induced by the inhomogeneous thermal fields.

It is found that the horizontal distribution of the initial potential temperature and its position relative to the mountain play important roles during the geostrophic adjustment and local frontogenesis. The frontogenesis is weakened by the mountain when the initial thermal perturbation is located at the base of the upwind slope. The frontal discontinuity cannot occur unless the horizontal contrast of the initial potential temperature is great enough. Whereas, the situation is opposite when the initial thermal disturbance is mainly situated near the peak of the mountain. Complementary to the aforementioned cases, the effect of topography on the frontogenesis depends on the stratification of the flow when the initial thermal disturbance lies at the foot of lee slope. For weak stratification, topography is favorable to the formation of frontal discontinuity, vice versa. This discrepancy is attributed to the difference of subsidence warming, caused by the mountain, when the stratification is either strong or weak.

Furthermore, the energy conversion ratio between the kinetic and potential energy during the geostrophic adjustment process is also affected by the topography. In contrast to the flat bottom case, the ratio is reduced (increased) when the initial thermal perturbation lies in the up-wind slope (lee slope). The reason is that the gravity force does negative work in the former case while does positive work in the latter case.

Key words: Topography, Geostrophic adjustment, Frontogenesis

1. Introduction

As far as we know, two kinds of frontal models have been proposed: one is the balanced frontal model introduced by Hoskins and Bretherton (1972), another is the unbalanced frontal model posed by Ou (1984), Blumen and Wu (1995) and Wu and Blumen (1995). The former can explain the most frontogenesis processes in the atmosphere that are influenced by the large scale forcing. While the latter describes the frontogenesis process through the geostrophic adjustment of an initial unbalanced flow instead of the large scale forcing (for simplicity, hereafter, call it geostrophic adjustment frontogenesis). This model can really catch some characteristic features of frontogenesis observationally. For example, Yu (1997) pointed out that, although there is no evident mesoscale convergence flow, the mesoscale convergence flow can be excited and formed the sea breeze front finally as long as the

①This work was supported by the National Natural Science Foundation of China under Grant 49735180, and by the State Key Basic Program: CHERES.

temperature difference between sea and land is large enough. Recently, Sanders (1999) analyzed a short-lived cold front that developed in Arizona on 26 March 1991. His results show that this frontogenesis was attributable mainly to the horizontal variation of the surface heat flux during the morning, with little heating in a region of dense cloud cover and scattered showers in the west and with intense heating in a region of only thin high clouds to the east. The different heating increased the horizontal gradient of temperature, which induced the ageostrophic circulation and then resulted in a collapse toward discontinuity. According to Blumen et al. (1996), the frontogenesis happened in Kansas area on 9 March 1992 was also a result of the geostrophic adjustment.

Since the unbalance frontogenesis model was put forward, many research papers have emphasized various aspects of this subject. Wang and Wu (1998) considered the effect of stratification on the frontal structure. Blumen (2000) and Fang and Wu (1998) analyzed the transient adjustment problem and determined the geostrophic adjustment frontogenesis conditions. For simplicity, all these works took the lower boundary as flat surface. Hsueh and Cushman-Roision (1983) and others had ever studied the topographic effect on frontogenesis in ocean. Making use of the approximate method, Wu (1996) discussed the geostrophic adjustment frontogenesis in the uniform potential vorticity flow with undulated bottom surface. After that, Wang et al. (2000), using the ARPS model, analyzed the influence of 3-dimensional topography on the geostrophic adjustment frontogenesis. Results show that the position of initial unbalanced flow relative to the mountain will produces a great impact on the geostrophic adjustment frontogenesis and the energy conversion ratio between kinetic and potential energy. Based on these heuristic works, an analytical model is used in this work to make further study on the topographic effect. For simplicity, this work is mainly focused on the geostrophic adjustment of an initial unbalanced flow that is a motionless flow with thermal perturbation.

This paper is organized as follows. The basic equations and method used in this work are presented in Section 2, Sections 3 and 4 discuss the topographic effect on the geostrophic adjustment and frontogenesis in the zero and uniform potential vorticity flow respectively, Section 5 summarizes the major results.

2. Basic equations

As Blumen and Wu (1995), the fluid is incompressible and stably stratified; the constant rotation rate is $f/2$, where f is the Coriolis parameter; and the motion is assumed to vary only in the (x,y) plane, where x is horizontally directed and z is directed upward anti-parallel to gravity g. If the initial wind field and the potential temperature field do not satisfy the thermal wind relation, then the geostrophic adjustment will take place. The adjustment process can be investigated by three basic principles: conservation of potential vorticity, absolute momentum, and potential temperature. They are

$$\frac{d}{dt}\left[\left(f+\frac{\partial v}{\partial x}\right)\frac{\partial \theta}{\partial z}-\frac{\partial v}{\partial z}\frac{\partial \theta}{\partial x}\right]=0\,, \tag{1}$$

$$\frac{d}{dt}(fx+v)=0\,, \tag{2}$$

$$\frac{d\theta}{dt} = 0 \ . \tag{3}$$

Here $d/dt = \partial/\partial x + u\partial/\partial x + w\partial/\partial z$, where t denotes time and (u,w) are (x,z) velocity component, while v is the horizontal wind that is normal to the x axis. The fluid is assumed to be unbounded in the horizontal direction with rigid surfaces at the bottom and upper boundary. To obtain the dimensionless equations, the following dimensional relations are introduced, where the prime notation denotes the dimensionless quantities

$$x = Lx' \ , \quad z = Hz' \ ,$$

$$(u,v) = U(u',v') = fL(u',v') \ ,$$

$$\theta = \Delta\theta\theta' \ .$$

As far as the mesoscale system in this work is concerned, the Rossby number $R_0 = \frac{U}{FL} \sim 1$. This implies $U \approx fL$, which has been used in the above equation. The dimensionless forms of (1)–(3) are

$$\frac{d}{dt}\left[(1+\frac{\partial v}{\partial x})\frac{\partial\theta}{\partial z} - \frac{\partial v}{\partial z}\frac{\partial\theta}{\partial x}\right] = 0, \tag{1'}$$

$$\frac{d}{dt}(x+v) = 0 \ , \tag{2'}$$

$$\frac{d\theta}{dt} = 0 \ . \tag{3'}$$

The prime notation has been dropped for brevity.

(1′)–(3′) can be expressed alternatively as

$$q(x,z) = (1+\frac{\partial v}{\partial x})\frac{\partial\theta}{\partial z} - \frac{\partial v}{\partial z}\frac{\partial\theta}{\partial x} = q_0(x_0,z_0) \ , \tag{4}$$

$$x+v = x_0 + v_0(x_0,z_0) \ , \tag{5}$$

$$\theta(x,z) = \theta_0(x_0,z_0) \ , \tag{6}$$

where the subscript 0 indicates the initial quantities.

It is convenient at this stage to introduce momentum coordinate X and the terrain-following coordinate Z

$$X = x+v, \quad Z = \frac{z-h}{1-h} \ , \tag{7}$$

where h denotes the topography and it is the function of x only. According to (5) and (6), we have

$$X = X_0 = x_0 + v_0 \ , \tag{8}$$

and

$$\theta(X,Z)=\theta_0(X_0,Z_0)=\theta_0(X,Z_0)\ . \tag{9}$$

Following the transformational relations between (X,Z) and (x,z), we can easily obtain

$$\frac{\partial v}{\partial x}=\frac{(1-h)\frac{\partial v}{\partial X}+(Z-1)\frac{\partial h}{\partial x}\frac{\partial v}{\partial Z}}{(1-h)(1-\frac{\partial v}{\partial X})}\ , \tag{10a}$$

$$\frac{\partial v}{\partial z}=\frac{\frac{\partial v}{\partial Z}}{(1-h)(1-\frac{\partial v}{\partial X})}\ , \tag{10b}$$

$$\frac{\partial \theta}{\partial x}=\frac{\left[1-h+(Z-1)\frac{\partial h}{\partial x}\frac{\partial v}{\partial Z}\right]\frac{\partial \theta}{\partial X}}{(1-h)(1-\frac{\partial v}{\partial X})}+\frac{Z-1}{1-h}\frac{\partial h}{\partial x}\frac{\partial \theta}{\partial Z}\ , \tag{10c}$$

$$\frac{\partial \theta}{\partial z}=\frac{\frac{\partial v}{\partial Z}\frac{\partial \theta}{\partial X}}{(1-h)(1-\frac{\partial v}{\partial X})}+\frac{1}{1-h}\frac{\partial \theta}{\partial Z}\ . \tag{10d}$$

Inserting (10a)–(10d) into (4), and after some lengthy manipulations, the potential vorticity q in (X,Z) can be read as

$$q=\frac{1}{1-h}\frac{\frac{\partial \theta}{\partial Z}}{1-\frac{\partial v}{\partial X}}=q_0\ . \tag{11}$$

The final state is characterized by the thermal wind balance, which may be expressed as

$$\frac{\partial v}{\partial Z}=(1-h)\frac{\partial \theta}{\partial X}-F\ , \tag{12}$$

where F is determined by the following relation:

$$F=(1-Z)\frac{\partial h}{\partial x}\frac{\partial \theta}{\partial Z}(1-\frac{\partial v}{\partial X})+(1-Z)\frac{\partial h}{\partial x}\frac{\partial \theta}{\partial X}\frac{\partial v}{\partial Z}\ . \tag{13}$$

Our problem is now to solve v and θ by virtue of (8), (9), and (11) and together with the assumption that the final state would be geostrophic. This approach has been used by Ou (1984), Blumen and Wu (1995), Hsueh and Cushman-roision (1983) and Wu (1995).

3. Zero potential vorticity flow (ZPV)

For simplicity, an extreme case showed in Fig.1 is considered first. The fluid is initially at rest so that there is no Coriolis force to balance the pressure gradient force that would then drive the cold fluid rightward to the warm side below the leftward warmer fluid. The Coriolis force acting on this transverse circulation would generate a vertical shear in the direction that

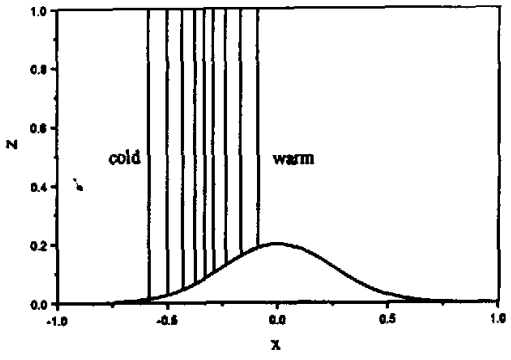

Fig. 1. Schematic drawing of the initial potential temperature field in the ZPV case.

crosses the stream, which tends to offset the pressure gradient force. The adjustment continues until the geostrophic balance is established and the fluid reaches a steady equilibrium. During this process, the undulated underlying surface surely exerts effects on the movement of the particle and results in some different results.

The initial conditions mentioned above may be depicted as

$$v_0(x_0,z_0)= 0 \ , \tag{14}$$

$$\theta_0 = \theta_0(x_0) \ . \tag{15}$$

In virtue of (14), Eq.(8) is simplified as

$$X= X_0 = x_0 \ . \tag{16}$$

The substitution of (14) and (15) into (4) leads to the fact that the potential vorticity is zero, i.e. $q= 0$. Whence the following equation follows immediately from the conservation principle of potential vorticity (11)

$$\frac{\partial \theta}{\partial Z} = 0 \ , \tag{17}$$

i.e. θ is only the function of X. Mathematically, (9) can be written as

$$\theta(X)= \theta_0(X_0)= \theta_0(x_0) \ . \tag{18}$$

Substituting (17) into (13), the thermal wind relation (12) reduces to

$$\frac{\partial v}{\partial Z} = (1- h)\frac{\partial \theta}{\partial X} - (1- Z)\frac{\partial h}{\partial x}\frac{\partial \theta}{\partial X}\frac{\partial v}{\partial Z} \ . \tag{12'}$$

From (7) we have $\frac{\partial v}{\partial Z} = -\frac{\partial x}{\partial Z}$. With this relation, (12') can be formulated as an equation of $\frac{\partial x}{\partial Z}$

$$\frac{\partial x}{\partial Z} = -[1- h(x)]\frac{d\theta}{dX} - (1- Z)\frac{d\theta}{dX}\frac{dh(x)}{dx}\frac{\partial x}{\partial Z} \ .$$

By introducing $\frac{\partial h}{\partial Z} = \frac{dh}{dx}\frac{\partial x}{\partial Z}$, and after some algebraic manipulation, we obtain

$$\begin{aligned}\frac{\partial x}{\partial Z} &= -\left[(1-Z)\frac{\partial h(x)}{\partial Z} + 1 - h(x)\right]\frac{d\theta}{dX} \\ &= -\left[(1-Z)\frac{\partial h(x)}{\partial Z} + \frac{\partial Z - Zh(x)}{\partial Z} + Z\frac{\partial h(x)}{\partial Z}\right]\frac{d\theta}{dX} \\ &= -\frac{\partial Z + (1-Z)h(x)}{\partial Z}\frac{d\theta}{dX} \ . \end{aligned} \tag{19}$$

Now, by integrating this equation with respect to Z, it follows the expression of x in the adjusted state

$$x = -\frac{d\theta}{dX}[Z + (1-Z)h(x)] + C(X) \ , \tag{20}$$

where $C(X)$ is an arbitrary function to be determined.

By using (7), (16) and (18), (20) can be expressed alternatively as

$$x = -\frac{d\theta_0}{dx_0}z + C(x_0) \ . \tag{20'}$$

This shows that the isentrope $\theta_0(x_0)$ in the adjusted state are straight with a slope that is inversely proportional to the lateral potential temperature gradient in the initial state. It is obvious that the larger $\left|\frac{\partial\theta_0}{\partial x_0}\right|$ is, the larger the angle the isentrope $\theta_0(x_0)$ tilts. This different inclination of the isentropes agrees with the physical reasoning that the regions of greater potential temperature gradient in the initial state are ones of greater dynamical imbalance, which results in greater inclination of the fluid column during the adjustment. The different inclination of the isentropes thus produces regions of convergence (divergence) at the leading (trailing) edges of the isentrope where the initial potential temperature gradient is greatest. This will increases (reduces) the potential temperature gradient there under the condition that the potential temperature is conservative.

The following part is devoted to determine the function $C(x_0)$ by making use of the approach proposed by Hoskins and Bretherton (1972). In Fig. 2, EF is at large enough x such that it is nearly unaffected by the disturbance during the adjustment. AB and CD indicate the position of isentrope $\theta = \theta_0(x_0)$ at the initial and adjusted state, respectively. Since the mass

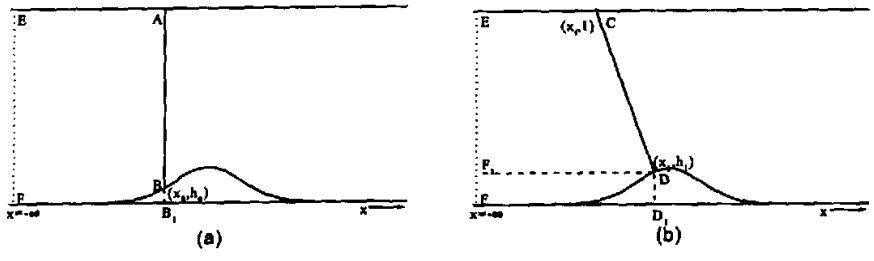

Fig. 2. Schematic drawing of the initial (a) and final position (b) of the isentrope $\theta = \theta_0(x_0)$.

is conservative, then the volume is also conservative, under the Boussinesq approximation. Thus we must have area($ABFE$)=area($C'DFE$), i.e.

$$1\cdot(x_0-x_{-1})-\int_{x_{-1}}^{x_0}h(\eta)d\eta=\frac{1}{2}[(x_1-x_{-1})+(x_1-x_{-1})](1-h_1)+h_1(x_1-x_{-1})-\int_{x_{-1}}^{x_1}h(\eta)d\eta \quad (21)$$

AB_1FE BB_1F CDF_1F DD_1FF_1 DD_1F

where (x_0,h_0) and (x_1,h_1) denote the initial and final position of fluid element on the mountain as shown in Fig. 2 and $\theta_0(x_0)$ is the potential temperature, $(x_r,1)$ represents the final position of the fluid element at the upper boundary. Substituting x_1 and x_r into (21), then we finally get

$$C(x_0)=\frac{1}{2}\frac{d\theta_0(x_0)}{dx_0}(1+h_1^2)+\int_{x_0}^{x_1}h(\eta)d\eta+x_0 \quad . \quad (22)$$

With the relation (22), (20′) becomes

$$x=\frac{1}{2}\frac{d\theta_0(x_0)}{dx_0}(1+h_1^2-2z)+\int_{x_0}^{x_1}h(\eta)d\eta+x_0 \quad . \quad (23)$$

This is essentially the same as (3.5) of Ou (1984) when the topographic effect is neglected. If we let z equal h_1 in (23), x_1 can be found as

$$x_1=\frac{1}{2}\frac{d\theta_0(x_0)}{dx_0}(1-h_1)^2+\int_{x_0}^{x_1}h(\eta)d\eta+x_0 \quad . \quad (23')$$

On the substitution of it into (23), we get the relation between x and (x_0,z) in the adjusted state, which delineates the isentrope $\theta_0(x_0)$ in the adjusted state. Naturally, the final geostrophic wind is obtained by using the relation $v=x_0-x$, which results from the combination of (7) and (16). These results are used to discuss the topographic effect on the geostrophic adjustment and frontogenesis.

3.1 *Topographic effect on geostrophic adjustment frontogenesis*

To illustrate the topographic effect, we take the unbalanced flow with the initial potential temperature $\theta_0=0.5\mathrm{erf}[1.93(x_0+0.1)]$ as an example. Figure 3 shows the cross section of the final state. It is clearly that the frontal discontinuity (Blumen and Wu, 1995) appears in both the wind and the potential temperature fields. However, as Blumen and Wu (1995) stated, the discontinuity, in such case, would not be observed with flat bottom. Evidently, this difference is ascribed to the topographic effect.

Following Hoskins and Bretherton (1972) and Blumen and Wu (1995), the Jacobian of transformation from (x,z) to (X,Z) space is used as an indicator of frontogensis. Based on (7) and (16), the Jacobian in our problem is given as

$$J=\frac{\partial x}{\partial X}[1-h(x)]=\frac{\partial x}{\partial x_0}[1-h(x)] \quad . \quad (24)$$

When J is not equal to zero, solutions are continuous and monotonous. While, the transform of coordinates is terminated when $J=0$. This means that the zero–order discontinuity in both velocity and potential temperature fields will form and it is considered as frontogenesis in the context of this model (Hoskins and Bretherton, 1972; Blumen and Wu, 1995). Since our interest is to study the topographic effect on the geostrophic adjustment frontogenesis, only the

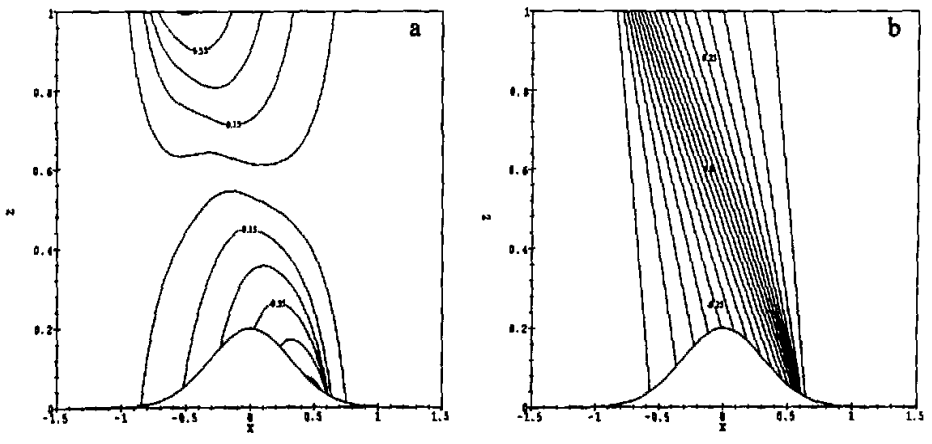

Fig. 3. Cross section of final states for zero potential vorticity flow. (a) velocity (b) potential temperature $h(x)= 0.2e^{-5x^2}$.

variation of J on the lower boundary is taken into account. Differentiating (23′) with respect to x_0 and inserting the result into (24), we get J at the bottom

$$J=\left[1-h_0+\frac{1}{2}\frac{d^2\theta_0}{dx_0^2}(1-h_1)^2\right]\Big/\left[1+\frac{d\theta_0}{dx_0}\frac{\partial h_1}{\partial x_1}\right]. \tag{25}$$

Obviously, the condition for $J= 0$, when the topographic effect is ignored, is

$$\left.\frac{d^2\theta_0}{dx_0^2}\right|_{\text{flat}} = -2\,. \tag{26′}$$

This is equivalent to the frontogenesis condition obtained by Blumen and Wu (1995). When the influence of topography is included, the value of J is not only determined by $d^2\theta_0 / dx_0^2$ but also depends on $d\theta_0 / dx_0$ and the initial and final positions of the fluid element at the lower boundary. Generally, the denominator in (25) does not equal zero when the slope of the mountain is not very steep. Consequently, J will be zero when the second derivative of the initial potential temperature satisfies the following relation

$$\left.\frac{d^2\theta_0}{dx_0^2}\right|_h = -\frac{2(1-h_0)}{(1-h_1)^2} = \frac{(1-h_0)}{(1-h_1)^2}\left.\frac{d^2\theta_0}{dx_0^2}\right|_{\text{flat}}. \tag{26}$$

If

$$\frac{1-h_0}{(1-h_1)^2} > 1\,, \tag{27}$$

then according to (26), the frontogenesis can only occur under the condition that

$$\left|\left.\frac{d^2\theta_0}{dx_0^2}\right|_h\right| > \left|\left.\frac{d^2\theta_0}{dx_0^2}\right|_{\text{flat}}\right|,$$

i.e. the discontinuity cannot appear unless the lateral variation of the initial potential temperature is larger than the case that the bottom is flat. In this sense, the topography hinders the frontal discontinuity from forming. Conversely, if

$$\frac{1-h_0}{(1-h_1)^2} < 1 \ , \tag{28}$$

then

$$\left| \left. \frac{d^2\theta_0}{dx_0^2} \right|_h \right| < \left| \left. \frac{d^2\theta_0}{dx_0^2} \right|_{\text{flat}} \right| \ ,$$

i.e. even though the lateral variation of the initial potential temperature is smaller compared to the case that the lower boundary is flat, the discontinuity may occur. So, the topography effect is favorable for the formation of frontal discontinuity. When the initial thermal perturbation is located at the base of the upwind slope or on the upwind slope (this means that h_0 is very small or, nearly zero), then the fluid element will climb up the mountain along the slope. If the mountain is wide enough that the fluid element still stay on the range of the upwind slope after the adjustment, then h_1 is always much larger than h_0. In this case, (27) is satisfied, then the topography is unfavorable for the frontogenesis. On the contrary, if the initial thermal perturbation lies near the peak of the mountain or on the lee slope (this implies h_0 is large), then the fluid element will flow down the slope under the effect of gravity. As a result, h_1 is much smaller than h_0. This satisfies the condition of (28). Thus, the mountain is favorable for the formation of discontinuity, and this case is shown in Fig. 3.

After qualitative analysis on the topographic effect, numeric results are given to illustrate the effect more directly. In the following example, the initial potential temperature is taken as

$$\theta_0 = \theta_0(x_0) = 0.5\text{erf}[1.93(x_0 + x_m)] \ , \tag{29}$$

where x_m is the point of maximum potential temperature gradient. It is used to denote the relative position between the initial disturbance and the mountain. Figure 4a shows the variation of the maximum value of $\frac{\partial\theta}{\partial x}$ at the adjusted state when the initial potential disturbance is situated at different position relative to the mountain. The mountain has no effect on the geostrophic adjustment when the initial thermal perturbation is far away from the mountain. The maximum value of $\frac{\partial\theta}{\partial x}$ is 6.86. As the initial thermal disturbance moves toward the mountain, the maximum value of $\partial\theta/\partial x$ is reduced gradually, the mountain hinders the frontogenesis, and the topographic effect is strongest when the initial unbalanced flow is at the foot of the upwind slope. After that, the maximum value of $\frac{\partial\theta}{\partial x}$ begins to increase little by little and reaches its maximum when $x_m = -0.34$. The mountain now plays an important role in increasing the potential temperature gradient. As $x_m \to -0.1$, the maximum value of $\frac{\partial\theta}{\partial x}$ tends to infinity and this implies the discontinuity forms. Beyond this point, the maximum value of $\frac{\partial\theta}{\partial x}$ decreases with the increase of x_m. However, it is still larger than 6.86, i.e. the mountain is still favorable for the formation of discontinuity.

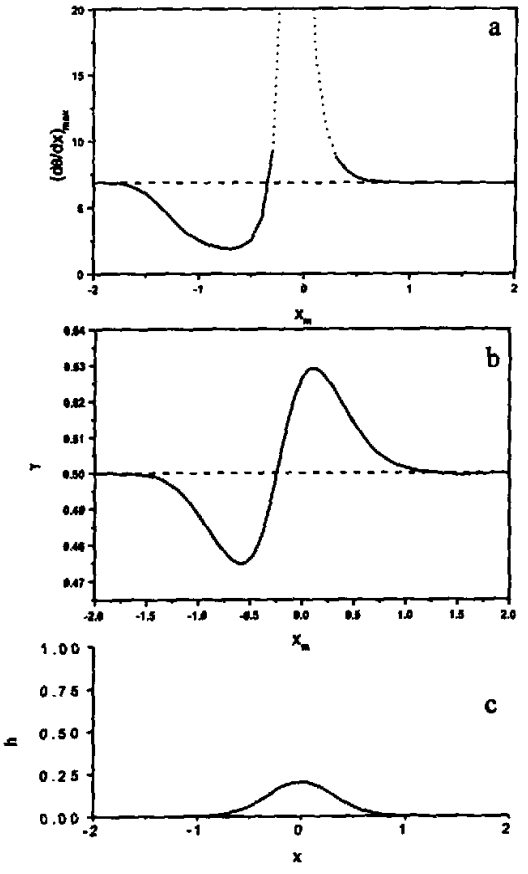

Fig. 4. The variation of $(\partial\theta / \partial x)_{max}$ at the bottom and energy conversion ratio γ with x_m. (a) $(\partial\theta / \partial x)_{max}$; (b) γ; (c) Height of the topography $h(x)= 0.2e^{-5x^2}$

To summarize based on the above analysis, if the initial thermal perturbation is located on the upwind slope or at the foot of the mountain, the topography is unfavorable for frontogenesis. The frontal discontinuity may appear only under the condition that the horizontal contrast of the initial potential temperature is great enough. However, when the initial thermal disturbance is mainly situated near the peak of the mountain, then the topographic effect is favorable for frontogenesis.

3.2 *Topographic effect on the energy conversion ratio*

Following Blumen and Wu (1995), the changes in kinetic and potential energy during the adjustment are

$$\Delta E_k = \frac{1}{2}\int_{-\infty}^{\infty}\int_0^1 v^2 JdXdZ = \frac{1}{2}\int_{-\infty}^{\infty}\int_0^1 v^2 Jdx_0 dZ \ . \tag{31}$$

and

$$\Delta E_p = -\int_{-\infty}^{\infty}\int_0^1 \theta[Z(1-h)+h](1-h)dXdZ + \int_{-\infty}^{\infty}\int_0^1 \theta[Z(1-h)+h]JdXdZ$$
$$= -\int_{-\infty}^{\infty}\int_0^1 \theta_0(x_0)[Z(1-h)+h](1-h)dx_0dZ$$
$$+\int_{-\infty}^{\infty}\int_0^1 \theta_0(x_0)[Z(1-h)+h]Jdx_0dZ \ . \tag{32}$$

For zero potential vorticity flow with flat bottom, Ou (1984), Blumen and Wu (1995) and Wu and Blumen (1995) established that the energy conversion ratio $\gamma(=\frac{\Delta E_k}{\Delta E_p})=\frac{1}{2}$. However, the ratio is modified when the influence of topography is considered. Figure 4b shows the variation of γ with x_m under the situation that the initial potential disturbance is given by (29). Obviously, γ is smaller than $\frac{1}{2}$ when the initial unbalanced perturbation lies on the upwind slope. While, when the initial perturbation is at the peak of the mountain or on the lee slope, γ is larger than $\frac{1}{2}$. These results are consistent with the physical reasoning. In the former case the gravity force exerts negative work and prevent the potential energy from converting to the kinetic energy. However, in the latter case, the gravity force does positive work and is beneficial to the release of potential energy and then increases the conversion ratio.

We will provide an alternative explanation for the topographic effect on frotogenesis as follows. In the case that the initial unbalance flow is on the upwind side of the mountain, the gravity force does negative work and inhibits the intension of the horizontal convergence and hence weakens the frontogensis process. While, if the initial unbalanced flow is on the lee slope side, the gravity force does positive work, which will strengthen the horizontal convergence and then increase the horizontal potential temperature gradient.

4. Uniform potential vorticity flow

In the last section, the topographic effect on geostrophic adjustment of zero potential vorticity flow is studied in length. However, the zero potential flow is merely an approximation for the atmosphere. To some extent, the non-zero potential flow is a much better approximation than the former.

By eliminating v and θ in (10) and (12), one gets

$$q(1-h^2)\frac{\partial^2\theta}{\partial X^2}+\frac{\partial^2\theta}{\partial Z^2}-q(1-h)\frac{\partial h}{\partial X}\frac{\partial\theta}{\partial X}-\frac{1}{q(1-h)}\frac{\partial}{\partial Z}[q(1-h)]\frac{\partial\theta}{\partial Z}=q(1-h)\frac{\partial F}{\partial X} \ , \tag{33}$$

$$q(1-h^2)\frac{\partial^2 v}{\partial X^2}+\frac{\partial^2 v}{\partial Z^2}+(1-h)\frac{\partial}{\partial X}[q(1-h)]\frac{\partial v}{\partial X}+\frac{1}{1-h}\frac{\partial h}{\partial Z}\frac{\partial v}{\partial Z}=(1-h)\frac{\partial}{\partial X}[q(1-h)]$$
$$-\frac{\partial F}{\partial Z}-\frac{1}{1-h}\frac{\partial h}{\partial Z}F \ . \tag{34}$$

Although (33) and (34) are complicated in form, they can be resolved, provided the potential vorticity is larger than zero, with the following procedures:

Step 1. Calculating F and h from the initial v and θ.

Step 2. Since q is larger than zero, (33) and (34) are elliptical type of partial differential equations that can be solved with SOR method under the proper boundary conditions. By

inserting the new value of θ gotten from (33) into (13), one obtains a new F. Then, on substitution of it into (34), velocity v is obtained by resolving (34).

Step 3. Introducing the new values of v and θ into (13) gives the new F again. Based on this and the transformation between the two coordinates systems, the distribution of the topography in the new coordinates is obtained.

Step 4. Repeating the above procedures, the proper solutions will be found as long as the topography is not very steep.

Further assuming that the unbalanced perturbation is confined within a limited area and the fluid particles initially located at the lower surface remain at the same surfaces during the adjustment, then the proper boundary conditions for (33) and (34) can be expressed as

$$\begin{cases} X \to \pm\infty, & \partial\theta / \partial X \to 0 \\ Z = 0, & \theta = \theta(X,0) = \theta_0(X_0, h(X_0)) \\ Z = 1, & \theta = \theta(X,1) = \theta_0(X_0,1) \end{cases}, \tag{35}$$

$$\begin{cases} X \to \pm\infty, & \partial v / \partial X \to 0 \\ Z = 0, & \dfrac{\partial v}{\partial Z} = \dfrac{(1-h(x))\dfrac{\partial\theta}{\partial X} - \dfrac{\partial h(x)}{\partial x}\dfrac{\partial\theta}{\partial Z}\left(1-\dfrac{\partial v}{\partial X}\right)}{1+\dfrac{\partial h(x)}{\partial x}\dfrac{\partial\theta}{\partial X}} \\ Z = 1, & \dfrac{\partial v}{\partial Z} = (1-h(x))\dfrac{\partial\theta}{\partial X} \end{cases}. \tag{36}$$

For simplicity, the initial unbalanced flow is assumed to be motionless and the potential temperature is as follows

$$\theta_0(x_0, z_0) = z_0 + 0.25\mathrm{erf}[4.18(x_0 - x_m)]$$

(x_m has the same meaning as it in the last section). Clearly, the initial potential vorticity is uniform through the domain, i.e. $q_0 = 1$. The essence of uniform potential vorticity is that the basic stratification of the atmosphere is considered. This is much closer to the real situation than the zero potential vorticity flow. The geostrophic solution in the case that $x_m = -0.1$ is shown in Fig. 5, in which the topography is taken as $h(x) = 0.15e^{-5x^2}$. The characteristic features displayed in Fig. 5a are almost the same as in Fig.4a. The frontal discontinuity appeas in the final velocity and potential vorticity fields.

Figure 6 gives the variation of the maximum value of $\partial\theta / \partial x$ at the adjusted state when the initial potential disturbance lies at the different position relative to the mountain. Compared with Fig. 4a, there is a remarkable characteristic in Fig. 6a. That is, when the initial thermal perturbation is located at the foot of the lee slope, the maximum value of $\partial\theta / \partial x$ is smaller than that in the case that the bottom is flat. This implies that the mountain inhibits the frontogenesis process. The reason is that, in this case, the topography nearly has no effect on the fluid in the warm side, while its effect on the motion of the fluid in the cold side is still large, which causes prominent subsidence warming and reduces the potential temperature contrast between cold and warm fluid. As a result, the horizontal convergence is greatly decreased, which leads to the smaller maximum value of $\partial\theta / \partial x$ in the adjusted state. However, in the zero potential vorticity flow, since the basic stratification of the atmosphere is neglected, the subsidence warming induced by the mountain is too weak to produce the notable variation of the pressure in the cold side. Consequently, the phenomenon appearing in uniform potential vorticity flow mentioned above does not occur.

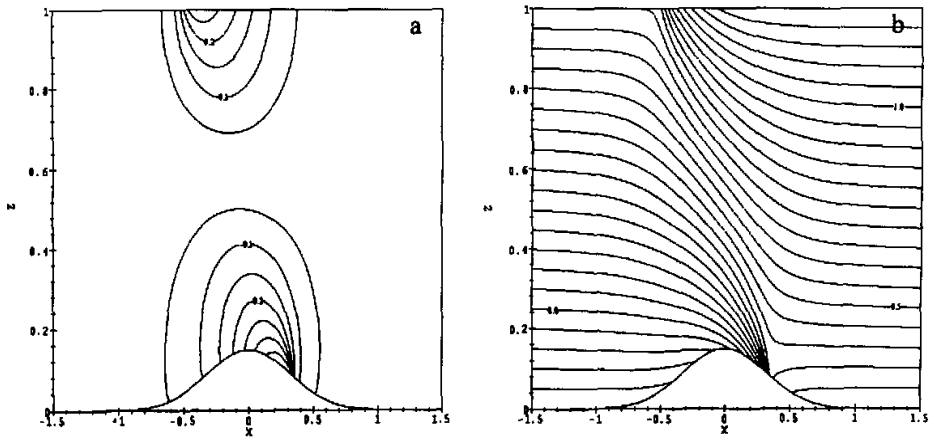

Fig. 5. Cross section of final states for uniform potential vorticity flow ($h(x)= 0.15e^{-5x^2}$). (a) velocity, (b) potential temperature.

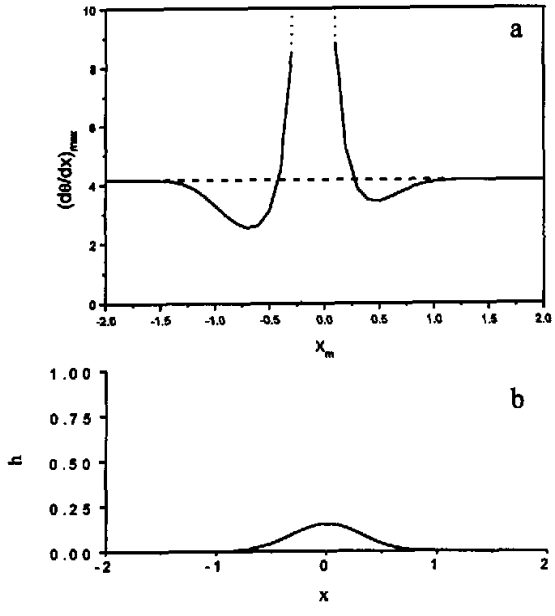

Fig. 6. The variation of $(\partial\theta / \partial x)_{max}$ at the bottom and energy with x_m. (a) $(\partial\theta / \partial x)_{max}$; (b) Height of the topography $h(x)= 0.15e^{-5x^2}$.

Like in the zero potential vorticity flow, the energy conversion ratio is also calculated for the uniform potential vorticity flow. The primary features are the same as in the zero potential

vorticity flow except that the ratio is a little smaller than that in the flat bottom situation when the initial unbalanced flow lies at the base of the lee slope. This difference is due to the subsidence warming effect.

5. Conclusion

The major motivation for this work is to study the topographic effect on the local frontogenesis and geostrophic adjustment caused by the horizontal difference of the thermal characteristics. It is found that the horizontal distribution of the initial potential temperature and its position relative to the mountain play important roles in the geostrophic adjustment and local frontogenesis. In the case that the initial thermal perturbation is located at the foot of the upwind slope, the frontogenesis process is weakened by the mountain. The frontal discontinuity occurs only under the condition that the horizontal contrast of the initial potential temperature is large enough. However, when the initial thermal disturbance is mainly situated near the peak of the mountain, the topographic effect is opposed to the former. Complementary to the aforementioned cases, the effect of topography on the frontogenesis depends on the stratification of the flow when the initial thermal disturbance lies at the foot of lee slope. For weak stratification, topography is favorable for the formation of frontal discontinuity, vice versa. This discrepancy is attributed to the difference of subsidence warming, induced by the mountain, when the stratification is either strong or weak.

In addition, the energy conversion ratio between the kinetic and potential energy in the geostrophic adjustment process is also affected by the topography. Compared with the flat bottom case, the ratio is reduced when the initial thermal perturbation lies on the upwind slope and is increased when the initial thermal perturbation is situated on the lee slope. The reason is that the gravity force does negative work in the former case while does positive work in the latter case.

Although the topographic effect on the local frontogenesis and geostrophic adjustment, induced by the horizontal difference of the thermal characteristics, is depicted by this work, the results are rather idealized. For example, the zero or uniform potential vorticity flow cannot well represent the real atmosphere features. Furthermore, only the final state can be obtained with the method used here. The detailed transient adjustment and frontogenesis process cannot be described. These problems should be improved to study the influence of topography in the future.

We are much grateful to Dr. Wang Yuan for his help in improving the readability of this paper. We also acknowledge the anonymous reviewers for their helpful comments and criticism on an earlier manuscript.

REFERENCES

Blumen, W., and R. Wu, 1995: Geostrophic adjustment: Frontogenesis and energy conservation. *J. Phys. Oceanogr.*, **25**, 428–438.

Blumen, W., 2000: Inertial oscillation and frontogenesis in a zero potential vorticity model. *J. Phys. Oceanogr.*, **30**, 428–438.

Blumen W. et al., 1996: The low-level structure and evolution of a dry arctic front over the central United States. Part II: Comparison with theory. *J. Atmos. Sci.*, **124**, 1676–1692.

Fang Juan, and Wu Rongsheng, 1998: Frontogenesis, evolution and the time scale of front formation. *Advances in Atmospheric Sciences*, **15**, 233–246.

Hoskins, B. J., and F. P. Bretherton, 1972: Atmospheric frontogenesis models: Mathematical formulation and solution. *J. Atmos. Sci.*, **29**, 11–37.

Ou, H. W., 1984: Geostrophic adjustment: A mechanism for frontogenesis. *J. Phys. Oceanogr.*, **14**, 994–1000.

Ou, H. W., 1986: On the energy conversion during geostrophic adjustment. *J. Phys. Oceanogr.*, **16**, 2203–2204.

Hsueh, Y., and B. Cushman-Roisin, 1983: On the formation of surface to bottom fronts over steep topography. *J Geophys. Res.*, **88**, 743–750.

Sanders, F., 1999: A short-lived cold front in the southwestern United States. 127, 2395.

Wang, Y. F., and R. Wu, 1998: The influence of stratification on frontogenesis caused by geostrophic adjustment. *Acta Meteorologica Sinica*, **12**, 374–381.

Wang Yunfeng, R. Wu, and Y. N. Pan, 2000: Evolution and frontogenesis of an imbalanced flow—the influence of vapor distribution and orographic forcing. *Advances in Atmospheric Sciences*, **17**, 256–274.

Wu, R., and W. Blumen, 1995: Geostrophic adjustment of a zero potential vorticity flow initiated by a mass imbalance. *J. Phys. Oceanogr.*, **25**, 439–4458.

Wu Rongsheng, 1996: Topographic effect on geostrophic adjustment and frontogenesis in atmosphere. *From Atmospheric Circulation to Global Change, Celebration of the 80 birthday of Professor Ye Duzheng*, Edited by IAP, 441–451.

Yu Enhong, 1997: *Sea–Land Breeze and Its Application*, China Meteorological Press.

地形对地转适应和锋生的影响

方 娟 伍荣生

摘 要

作者的目的是分析地形对由于热力差异所引起的局地锋生现象和地转适应过程的影响。为此，分别用零位涡流和均匀位涡流来近似代替实际大气，并借助位涡、绝对动量、位温的守恒关系，就地形对适应锋生和适应过程中能量转换等问题进行了简单讨论。初始位温扰动的水平分布及其相对于地形的位置对适应锋生有重要影响。当初始热力扰动主要位于地形迎风坡山脚时，地形不利于锋面形成，这时要形成锋面不连续，初始位温梯度的水平变化必须非常显著；当初始热力扰动主要位于山顶附近时，地形促进流体运动的辐合，有利于锋面不连续的形成，这时即使初始位温梯度的水平变化不是很大，也可能会形成锋面；当初始热力扰动主要位于背风坡时，地形是否有利于锋面不连续的形成取决于流体的层结情况，如果流体的基本层结很弱，地形促进锋面不连续的形成，反之，地形不利于锋面不连续的形成，这种差异主要是由于在这两种情况下，地形引起的下沉增温效应的强弱是不同的。另外，地形对地转适应过程中动能和位能之间的能量转换率也有影响，与没有地形的情况相比，当初始热力差异显著区位于迎风坡时，能量转换率减小，当不平衡场位于背风坡时，能量转换率增加，原因是在迎风坡流体要克服重力作功，在背风坡重力对流体作正功。

关键词：地形，地转适应，锋生